DOI: https://doi.org/10.36094/sc.v89.2025.A_Study_on_Electrical_Properties_of_Ytterbium.Thejas.49

ARTICLE

Sci. and Cult. 91 (1–2) : 49-55 (2025)

A STUDY ON ELECTRICAL PROPERTIES OF YTTERBIUM OXIDE DOPED $Ba(Zr_{0.02}Ti_{0.98})O_3$ CERAMICS

T.S. THEJAS[1,2], B. SAHOO[1,2] AND P.K. PANDA*[1,2]

Ytterbium oxide (Yb_2O_3) (0.02-0.06 wt. %) doped Ba ($Zr_{0.02}Ti_{0.98}$) O_3 were synthesized by mixed oxide route. The powders were calcined at 1100 °C for 4 h, de-agglomerated, granulated pressed into pellets, and sintered at 1450 °C for 2 h. The samples were electrode with silver-palladium paste, cured at 1000 °C for 1 h, poled and characterized. Maximum piezoelectric coefficient (d_{33}) achieved was 345 pC/N and relative dielectric constant (K=14051.2) obtained at Curie temperature (T_c) and 100 Hz frequency for 0.02 wt.% Yb_2O_3 doping. This sample exhibits a higher positive strain of 0.46% at an electric field of 20.94 kV/cm could be a suitable lead-free piezo material for high strain and actuation application.

Keywords: *Yb_2O_3-doped BZT; lead-free piezoceramics; piezoelectric charge coefficient; Curie temperature.*

Introduction

In recent years, smart materials are widely used in numerous applications ranging from automotive industries to aerospace sector[1-7]. In the race of smart materials, perovskite-type titanate-based ceramics certainly stand at front from many years because of their exceptional ferroelectric, piezoelectric and dielectric properties[8]. $BaTiO_3$ (BT) is one of the members of this perovskite family discovered during World War-II and known to have the first ferroelectric ceramics prepared in the laboratory with viable electrical properties[9]. Barium Zirconate Titanate (BZT) a modified barium titanate system is gaining more attention in recent days due to possibilities to alter its electrical properties by changing titanium and zirconium ratio[10]. This interest is driven by the notable characteristics of Zr^{4+} ions, which include a high dielectric constant and low dielectric loss. Even high piezoelectric properties were obtained for Barium Calcium Zirconate Titanate (BCZT) ceramics by varying Zr^{4+} concentration[11]. The majority of investigations are centered on the preparation, microstructure, and dielectric characteristics of BZT ceramics. Also, BZT is lead free in nature, therefore, eliminates toxicity concerns unlike in Lead Zirconate Titanate (PZT) based piezo ceramics[12].

A number of researchers have communicated that the introduction of rare earth ion enhances the dielectric characteristics of BZT ceramics[13-18]. This improvement is attributed to their ability to exhibit low leakage current and low electric field. Modifications in the composition of BZT ceramics through rare earth doping have been explored by two approaches: 'donor-doping,' employing an anionic compensation mechanism that generates cationic vacancies and defects, thereby altering properties; and 'acceptor-doping,' aimed at further enhancing material performance[19, 20]. Rare-earth elements found to be used for altering the electronic properties of barium titanate[21, 22]. Recently a study on Sm_2O_3 doped BZT reported with improved dielectric and strain properties[23]. Most investigations on effects of rare earth doping in BZT

1 Materials Science Division, CSIR-National Aerospace Laboratories, Bengaluru 560017, India

2 Academy of Scientific and Innovative Research, Ghaziabad 201002, India

* Corresponding Author: pkpanda64@rediffmail.com

ceramics are explored on the structural, dielectric, relaxor and electrical properties. However, there is no study revealed regarding the piezoelectric as well as strain properties using ytterbium oxide (Yb_2O_3) as dopant in $Ba(Zr_{0.02}Ti_{0.98})O_3$ composition. Therefore, in the present paper, an effort is made to study the effect of electrical properties as well as strain properties on Yb_2O_3 doped BZT.

Experimental Section

Materials: High purity grade barium carbonate (99.9%), zirconia powder (99.8%), titania powder (99.95%), Ytterbium oxide (99.9%) were used as starting raw materials for preparation of the compositions.

Preparation of Powders: Ytterbium oxide (Yb_2O_3) doped BZT with composition $BaZr_{0.02}Ti_{0.98}O_3$- x wt. % Yb_2O_3 (x= 0, 0.02, 0.04, 0.06) was prepared by solid state reaction method. 20 grams batch of each composition was prepared using the above raw materials in stoichiometric amount. The powder mixture was wet milled using ethyl alcohol and zirconia ball (5 mm dia.) grinding media for 72 h. The powder slurry was dried, removed the zirconia grinding media and the dried powders were calcined in a furnace at 1100ºC for 4 h. The calcined powders were again wet milled for 72 h and dried. The dried powders were sieved to separate out the grinding media.10 grams of the dried powders were taken in a pestle mortar, mixed with 1.5 cc of 2% Polyvinyl Alcohol (PVA) solution and slowly grounded to form granules. 1.5 grams of granules were taken and pellets (12 mm in diameter) were prepared using a die and punch by applying pressure of 45kN for 10 minutes with the help of a hydraulic press. The above procedure is followed for preparation of pellets for all the four compositions. The pellets of all four compositions were sintered at 1450°C for 2h in a high-temperature furnace. The sintered pellets were levelled, polished and their top and bottom surfaces were coated with high temperature curing silver-palladium (Ag-Pd) alloy paste for electroding and cured at 1000°C for 1 h. Finally, the pellets were poled at 2kV/mm DC electric field, and their electrical properties were measured.

Characterization

X-ray diffraction patterns of the prepared samples were measured using D8 Focus, Bruker XRD machine. The electron micrographs of the sintered, polished and thermal etched samples were done using an electron microscope (Zeiss, UK). The d_{33} and d_{31} of the poled samples were measured using a piezo-meter (Model PM-35, M/s. Take control, UK). The dielectric properties of the pellets were measured with an impedance analyzer (6500B, Wayne-Kerr Electronics, UK), ferroelectric and strain properties were measured using a ferroelectric hysteresis loop tester (Radiant technology, USA).

Results and Discussion

Density Analysis: Densities of levelled, polished, ultrasonically cleaned sintered samples were measured by dimensional method. The relative densities of the undoped and Yb_2O_3-doped BZT samples with respect to theoretical density of BZT (5.85 g/cc) is depicted in Fig. 1. The graph shows addition of 0.02 wt. % of Yb_2O_3 to BZT resulted in a higher sintered density of 96.21%. The density further decreased with addition of higher wt.% of Yb_2O_3 doping. It could be due to larger grain size of 0.02 wt. % of Yb_2O_3 to BZT with less grain boundaries which contributed higher density of sample as observed from the SEM micrographs. Theoretical density of BZT is considered as 5.85 g/cc as reported elsewhere[24]. The increase in density for 0.02 wt. % of Yb_2O_3 to BZT also attributed to the higher density of Yb_3O_3 (9.17 g/cc) compared to ZrO_2 (5.68 g/cc) and BaO (density: 5.72 g/cc), but the density decreased further with increase in Yb_2O_3 doping could be due to smaller grain size with more grain boundaries.

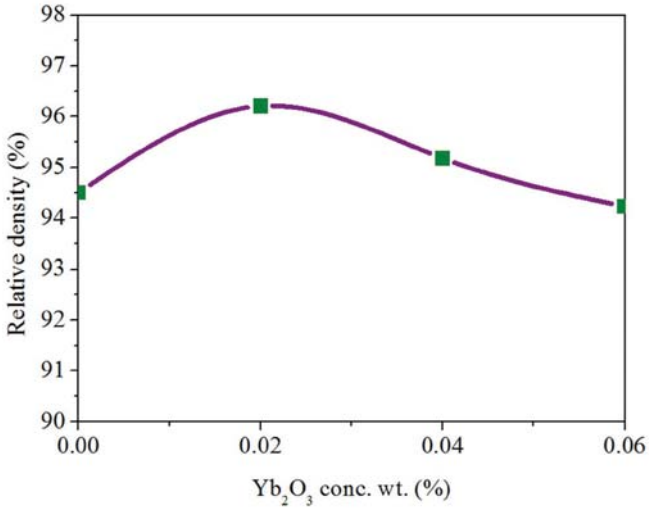

Fig. 1: Relative density of Yb_2O_3 doped BZT pellets.

XRD and Microstructural Characterization: The X-ray diffraction lines of the pellets with various wt. % Yb_2O_3 doped BZT samples are depicted in Fig. 2. A single-phase perovskite structure with no secondary phases were detected for all the compositions. XRD data obtained were compared with reported data of perovskite structure of tetragonal phase (JCPDS File No.89-1428 and perovskite cubic phase (JCPDS File No.89-2475) of base composition barium titanate[25]. In all these four compositions, cubic phase was dominated and hence tetragonal splitting could

not be observed. XRD plot also show shifting of peak position towards lower 2 theta angle with increase in Yb_2O_3 concentration which reflects an increase in lattice parameters with addition of the dopant. This reveals that Yb^{3+} ions were diffused into the $Ba(Zr_{0.02}Ti_{0.98})O_3$ structure and formed a homogenous solid solution. Similar observations were made by Li et al.[26].

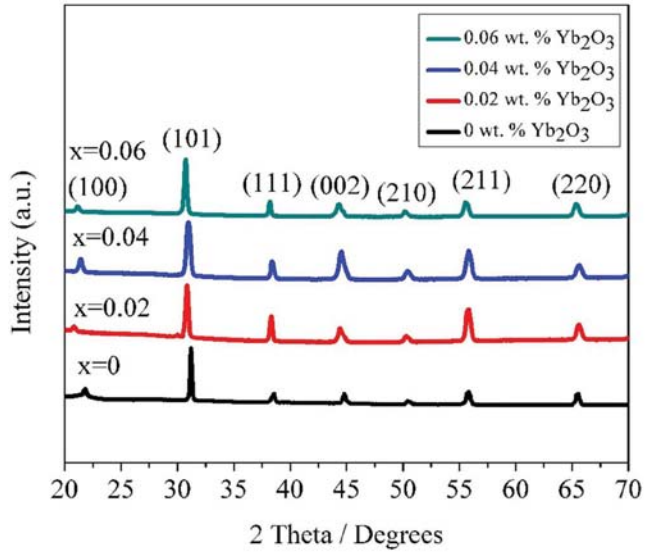

Fig. 2: XRD patterns of pure and Yb_2O_3 doped BZT pellets.

SEM micrographs of sintered BZT samples are presented in Fig. 3. The growth of grains appears to be constrained, leading to a reduction in grain size when more amount of rare-earth ion was introduced. The results showed that average grain size increased up to 0.02 wt. % Yb_2O_3, thereafter it decreased (Fig. 4). This reduction could be due to the dissolution of Yb^{3+} ions as dopants in the perovskite lattice, which may increase oxygen vacancies and contribute to overall cationic transport, thus reducing the grain size[27]. A similar decrease in grain size due to the incorporation of rare earth elements has been reported in the literature[28].

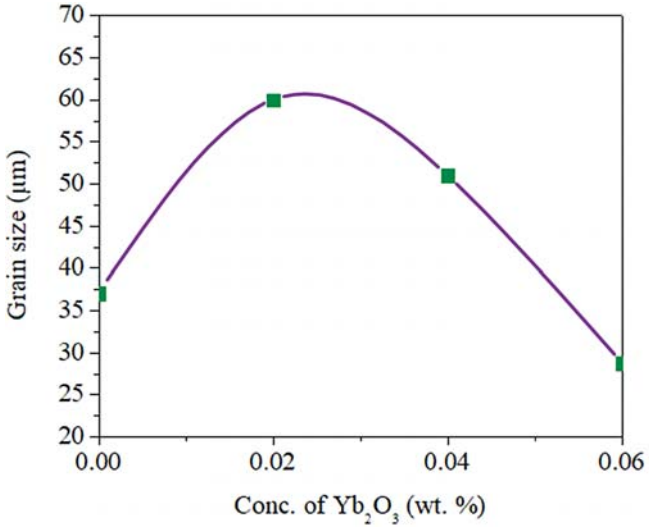

Fig. 4: Plot of average grain size of Yb_2O_3 doped BZT samples

Dielectric Properties: Dielectric constant vs. temperature graph of pure and Yb_2O_3 doped BZT at different frequencies are presented in Fig. 5. Highest dielectric constant of 14051.2 was obtained for 0.02 wt. % Yb_2O_3 doped BZT at Curie temperature (T_c) and at 100 Hz. As the Yb_2O_3 content increased, the maxima in *K* gradually decreased. The decline in K value at higher Yb_2O_3 concentration is attributed to decrease in grain size of the samples as the dielectric constant generally increased with increase in grain size[29, 30]. T_c of the pure BZT sample was found to be 125°C. It decreases to 123°C for 0.02 wt. % Yb_2O_3 doped BZT and declined further to 119°C for 0.06 wt. % Yb_2O_3 doped BZT. The effects are most likely due to the substitution of Yb^{3+} ions of different size in place of the host cations in the perovskite lattice which created B-

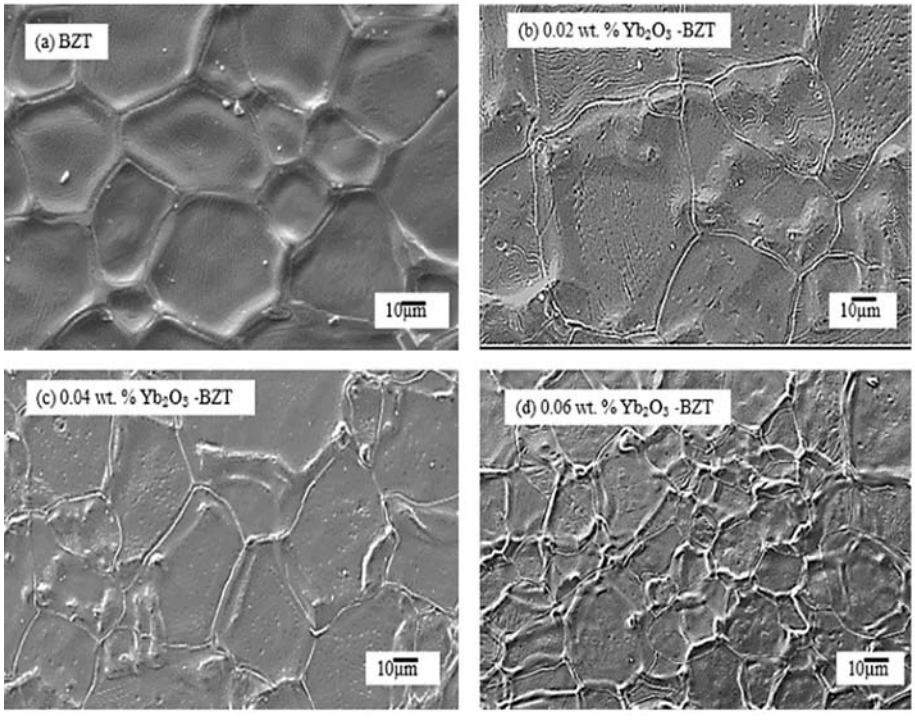

Fig. 3: SEM micrographs of (a) pure BZT (b) 0.02 (c) 0.04 (d) 0.06 wt. % Yb_2O_3 doped BZT.

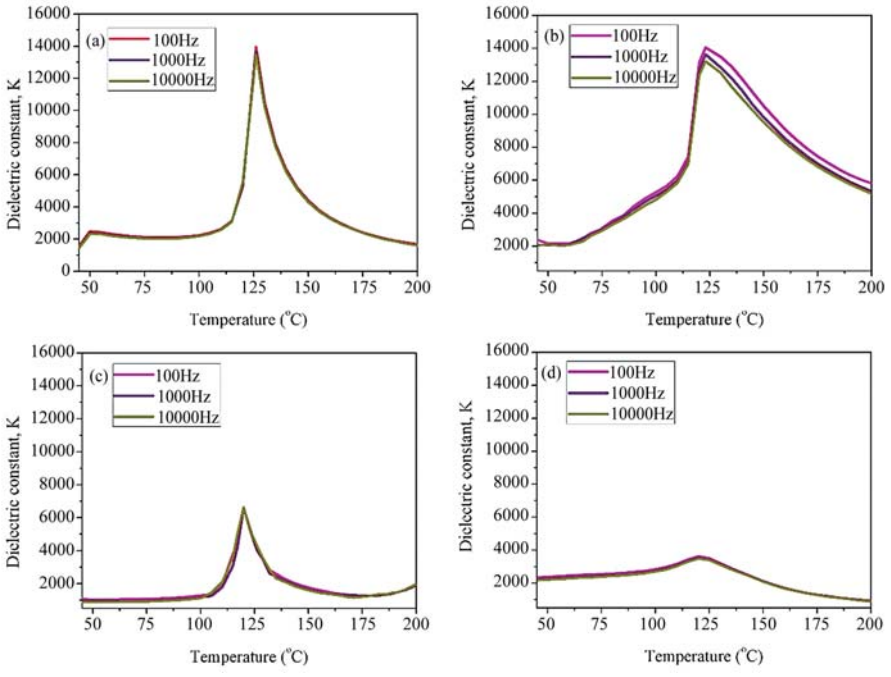

Fig. 5: Dielectric constant vs. temperature graph of (a) Pure BZT (b) 0.02 Yb_2O_3 wt.% doped BZT (c) 0.04 Yb_2O_3 wt.% doped BZT (d) 0.06 Yb_2O_3 wt.% doped BZT sample at 100 Hz, 1000 Hz, 10000 Hz.

site vacancy defects. It is reported that the ionic radii of Ba^{2+} in 12 coordinates is 0.161 nm, and Ti^{4+} or Zr^{4+} in 6 coordinates are 0.0605 nm or 0.072 nm, respectively and for Yb^{3+} , the ionic radii are 0.107 nm in 12 coordinates and 0.086 nm in 6 coordinates[15]. The variation in ionic radius of the doping ion Yb^{3+} probably induce the distortion of crystal lattice, thereby, increases the short-range harmonic force to compensate the long-range electrostatic force overall resulted a decrease in T_c values[31]. Table 1 shows the different electrical properties observed for Yb_2O_3 doped BZT. The highest dielectric constant value of 2148.7 among the four compositions was measured for 0.02 Yb_2O_3 wt. % doped BZT at room temperature (RT) are tabulated in Table 1.

Piezoelectric Properties: The piezoelectric charge coefficient (d_{33}) of Yb_2O_3 doped BZT sintered and poled pellets are shown in Fig. 6. Maximum d_{33} of 345 pC/N was obtained for 0.02 wt. % Yb_2O_3-doped BZT, then the value was decreased with increase in Yb_2O_3 content. d_{31} (Fig. 6) and electromechanical coupling factor (k_p) (Fig. 7) of the samples were followed a trend similar to d_{33}. Maximum value of d_{31} and k_p were found to be 108 pC/N and 0.542 for 0.02 wt. % Yb_2O_3 doped BZT respectively. Piezoelectric properties of a material solely depend on two major effects i.e. extrinsic and intrinsic effects. Effect from grain size, orientation and morphotropic phase boundary (MPB) said to be the intrinsic component of the piezoelectric constant in a sample[32, 33], whereas, 180 degree and 90-degree domain wall motion in the sample contributed the extrinsic component [34-36]. The improvement in piezoelectric properties (d_{33} and d_{31}) and electromechanical coupling factor (k_p) at 0.02 wt. % Yb_2O_3 can be attributed to the collaborative and combined effects arising from these extrinsic and intrinsic factors. The large grain size for this sample with less grain boundaries helped in effective poling vis-a-vis better alignment of dipoles in the direction of applied electric field which was reflected in higher piezoelectric properties. The decrease in the

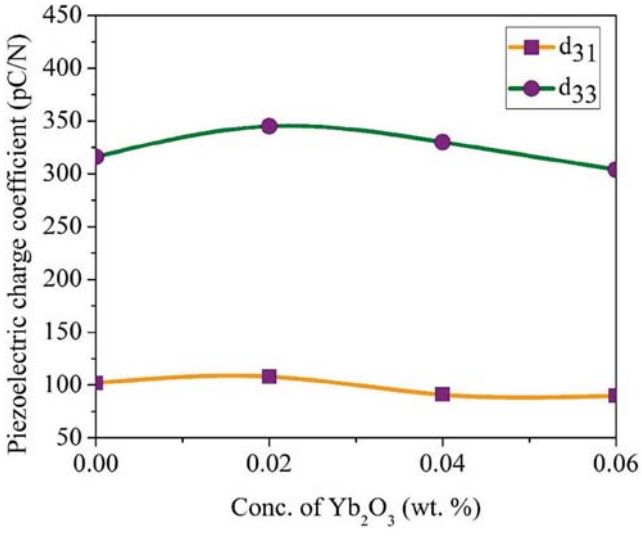

Fig. 6: Piezoelectric charge coefficients of Yb_2O_3 doped BZT pellets.

Table 1. Properties of Yb_2O_3 doped BZT pellets

Yb_2O_3 (wt. %)	Relative density (%)	d_{33}(pC/N)	d_{31}(pC/N)	Dielectric constant (*K*) at RT	Dissipation factor (tan δ) at RT	k_p
0.00	94.46	316	102	1389.21	0.017	0.541
0.02	96.21	345	108	2148.70	0.013	0.542
0.04	95.18	330	91	1888.80	0.026	0.502
0.06	94.23	304	79	1046.50	0.048	0.489

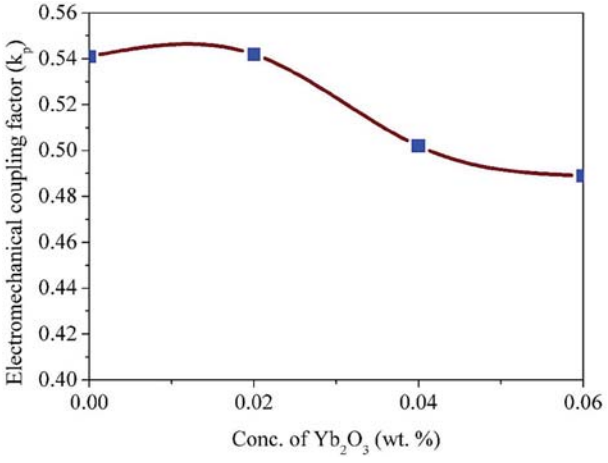

Fig. 7: Electromechanical coupling factor (k_p) of Yb_2O_3 doped BZT pellets.

piezoelectric coefficient with increase in dopant concentration after 0.02 wt.% is attributed to the decrease in the grain size and hence reduced the domain wall motion, thereby, decreased the piezoelectric properties[37, 38].

Hysteresis Loop Characterization: The *P–E* hysteresis loop of pellets is presented in Fig. 8. Maximum value of remnant polarization (P_r) was found to be 13.06 μC /cm^2 for 0.02 wt. % Yb_2O_3 doped BZT and decreased with increase in Yb_2O_3 concentration as shown in Table 2. With an increase in grain size, there was a corresponding increase in domain size, leading to a decrease in domain boundary[39,40]. This, in turn, results an increased contribution to polarization switching from extrinsic effects such as domain wall motion, consequently affecting the observed remnant polarization[41]. The decrease in P_r and increase in coercive field (E_c) can be attributed to the increase in hysteresis loss indicated by the increase in size of the hysteresis loop with increment in dopant (Yb_2O_3) concentration. Lower concentration (0.02 wt. %) of Yb_2O_3 exhibit low coercive fields, indicating that these materials are "soft" ferroelectrics that can be readily polarized by a weak electric field, and later tend to be "hard" due to increase in E_c with increase in Yb_2O_3 concentration.

Table 2. Hysteresis properties of Yb_2O_3 doped BZT pellets.

Compositions	P_r (μC/cm^2)	E_c (kV/cm)
$Ba(Zr_{0.02}Ti_{0.98})O_3$	12.80	2.60
$Ba(Zr_{0.02}Ti_{0.98})O_3$-0.02 wt.% Yb_2O_3	13.06	6.30
$Ba(Zr_{0.02}Ti_{0.98})O_3$-0.04 wt.% Yb_2O_3	12.98	6.60
$Ba(Zr_{0.02}Ti_{0.98})O_3$-0.06 wt.% Yb_2O_3	12.14	8.39

Strain Characterization: Fig. 9 illustrates the graph of electric field versus strain (%), for varying weight percentages (0, 0.02 wt.%, 0.04 wt.%, 0.06 wt.%) of Yb_2O_3-doped BZT. The graph shows a maximum strain of 0.46% for 0.02 wt.% Yb_2O_3 doped BZT at an electric field strength

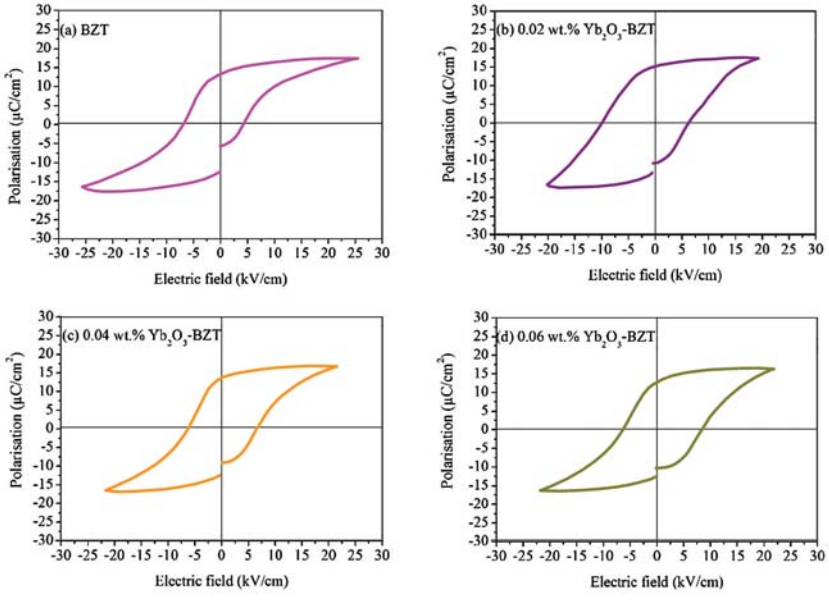

Fig. 8: Hysteresis loops of various wt. % Yb_2O_3 added BZT pellets.

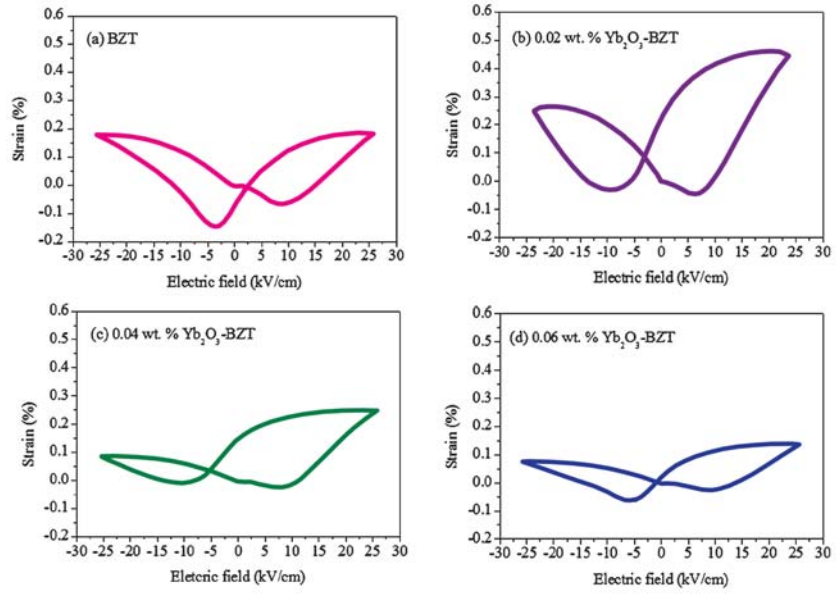

Fig. 9: Bipolar strain responses of Yb_2O_3 doped BZT pellets.

of 20.94 kV/cm. Strain in lead-free piezo materials induced by the asymmetric nature of crystal lattice which was further enhanced by addition of dopants[42,43]. The bipolar loop depicted in the graph illustrates that high displacement achieved when the sample was subjected to positive electric field compared to the displacement obtained by applying negative electric field. The asymmetric nature of strain curve would arise due to the development of internal bias field (E_{bias}) induced by charge carrier agglomeration at grain boundaries as modeled and reported by Yao et al.[44]. As per their model, at grain boundaries, the polarization vectors of domains in neighboring grains cannot compensate each other due to crystallographic mismatch. This leads to the occurrence of strong, locally varying depolarization fields (s+ and s-) at grain boundaries. So, free charge carriers in the vicinity shall be re-distributed to compensate the local depolarization fields. This agglomeration of free charges forms a local bias field (E_{bias}) in each grain, which has the same orientation as the applied electric field. The superposition of all these local bias fields leads to the macroscopically observable shift of the strain loop and can be seen as the source for the asymmetry nature in the strain curve.

Conclusions

The effect of Yb_2O_3 on the dielectric, piezoelectric, ferroelectric, and strain characteristics of $Ba(Ti_{0.98}Zr_{0.02})O_3$ was investigated. X-ray diffraction (XRD) patterns of the samples confirmed formation of phase-pure perovskite structure. Surface morphology of thermally etched samples reflected an increase in grain size up to 0.02 wt. % Yb_2O_3 doping and thereafter decreased. The highest density (96.21 %) of the sample was achieved for 0.02 wt. % Yb_2O_3 doping ascribed to a uniform microstructure with large grain size. Maximum d_{33} of 345 pC/N was obtained for 0.02 wt. % Yb_2O_3-doped BZT, then the value decreased with increase in Yb_2O_3 content. d_{31} and electromechanical coupling factor (k_p) of the samples were followed a trend similar to d_{33}. Maximum value of d_{31} and k_p were found to be 108 pC/N and 0.542 for 0.02 wt. % Yb_2O_3 doped BZT respectively. A maximum strain of 0.46% was observed for $Ba(Ti_{0.98}\ Zr_{0.02})O_3$ ceramics doped with 0.02 wt.% Yb_2O_3 at a relatively lower electric field of 20.94 kV/cm. Considering its high piezo and strain properties the sample is suitable for sensing and actuation application.

Acknowledgements

The authors extend thanks to XRD and SEM group of MSD, CSIR–NAL. Mr. T.S. Thejas thanks AcSIR, Ghaziabad for his enrolment as a Ph. D. student. Financial support of mission mode project (HCP-0036) CSIR, New Delhi is also acknowledged. ❐

References

1. D. Damjanovic, *Curr. Opin. Solid State Mater. Sci.* 3, 469–473 (1998).
2. S. Zhang, F. Yu, *J. Am. Ceram. Soc.* 94, 3153–3170 (2011).
3. H. Weng, F. Duan, Z. Ji, X. Chen, Z. Yang, Y. Zhang, B. Zou, *Ceram. Int.* 46, 3600–3605 (2020).
4. S.R. Anton, H.A. Sodano, *Smart Mater. Struct.* 16, R1–R21(2007).
5. A. Kumar, B. Purohit, P.K. Maurya, L.M. Pandey, P. Chandra, *Electroanalysis* 31, 1615–1629 (2019).
6. H. Elahi, K. Munir, M. Eugeni, M. Abrar, A. Khan, A. Arshad, P. Gaudenzi, *Integrated Ferroelectrics*, 211, 25–44 (2020).
7. S. Deka, V. Saxena, A. Hasan, P. Chandra, LM. Pandey, *Mater. Sci. Eng. C* 92, 932–941 (2018).
8. P.K. Panda, B. Sahoo, M Chandraiah, S. Raghavan, B. Manoj, J Ramakrishna, P Kiran, *J. Electron. Mater.* 44, 4349–4353 (2015).
9. B. Jaffe, H. Jaffe, W.R. Cook, Piezoelectrics Ceramics, Academic Press Inc., London, 1971.
10. J. Peng, D. Shan, Y. Liu, K. Pan, C. Lei, N. He, Z. Zhang, Q. Yang, npj Comput. Mater. 4, 66 (2018).
11. P.K. Panda, B. Sahoo, V. Sureshkumar, E. D. Politova, *J. Adv. Dielectr*. 11, 2150024 (2021).
12. P.K. Panda, *J. Mater. Sci.*, 44, 5049–5062 (2009).
13. D. Shan, Y. F. Qu, J. J. Song, *Solid State Commun.* 141, 65–68 (2007).
14. T. Badapanda**,** S. Sarangi, B. Behera, S. Anwar, T.P. Sinha, R. Ranjan, G.E. Luz Jr, E. Longo, L.S. Cavalcante, *J. Mater. Sci.: Mater. Electron.* 25, 3427–3439 (2014).
15. Y. Wang, L. Li, J. Qi, Z. Gui, *Ceram. Int.* 28, 657–661 (2002).
16. W. Li, Z. Xu, R. Chu, P. Fu, P., *Ceram. Int.* 38, 4353–4355 (2012).
17. S. B. Reddy, M.S.R. Rao, K. P. Rao, *Appl. Phys. Lett.* 91, 022917 (2007).
18. D.Y. Lu, M. Toda, M. Sugano, *J. Am. Ceram. Soc.* 89, 3112–3123 (2006).
19. K. Aliouane, A. Guehria-Laidoudi, A. Simon, J. Ravez, *Solid State Sci.* 7, 1324–1332 (2005).
20. F. Moura, A.Z. Simões, L.S. Cavalcante, M. Zampieri, J.A. Varela, E. Longo, M.A. Zaghete, M.L. Simões, *Appl. Phys. Lett.* 92, 032905 (2008).
21. X. Diez-Betriu, J.E. Garcia, C. Ostos, A.U. Boya, D.A. Ochoa, L. Mestres, R. Perez, *Mater. Chem. Phys.* 125, 493-499 (2011).
22. Y. Meng, K. Liu, X. Zhang, X. Lei, J. Chen, Z. Yang, B. Peng, C. Long, L. Liu, C. Li, *J. Am. Ceram. Soc.* 105, 5725–5737 (2022)
23. T. S. Thejas, B. Sahoo, P. K. Panda, *Phase Transit.*, 96, 434–445 (2023).
24. https://www.samaterials.com/barium-zirconate-titanate.html
25. Ch. S. Devi, M. B. Suresh, G. S. Kumar, G. Prasad, *J. Adv. Dielectr*. 2, 1250001 (2012).

26. Y. Li, R. Wang, X. Ma, Z. Li, R. Sang, Y. Qu., *Mater. Res. Bull*. 149, 601–607 (2014).
27. S. Shirasaki, H. Yamamura, H. Haneda, K. Kakegawa, J. Moori, *J. Chem. Phys*. 73, 4640–4645 (1980).
28. W. Yang, Y. Pu, X. Chen, J. Wang, *J. Phys. Conf. Ser.* 152, 012040–012045 (2009).
29. V. R. Mudinepalli, L. Feng, W. C. Lin, B. S. Murty, *J. Adv. Ceram*. 4, 46 (2015).
30. X. G. Tang, H. L. W. Chan, *J. Appl. Phys*. 97, 034109 (2005).
31. X. Chou, J. Zhai, H. Jiang, X. Yao, *J. Appl. Phys*. 102, 084106 (2007).
32. S. Tsurekawa, K. Ibaraki, K. Kawahara, T. Watanabe, *Scr. Mater* 56, 577–580 (2007).
33. Y. Chang, Z. Yang, L. Wei, *J. Am. Ceram. Soc*. 90, 1656–1658 (2007).
34. S. Dash, D. K. Pradhan, S. Kumari, Ravikant, M. M. Rahaman, C. Cazorla, K. Brajesh, A. Kumar, R. Thomas, P. D. Rack, D. K. Pradhan, *Phys. Rev. B* 104, 224105 (2021).
35. P. K. Panda, B. Sahoo, T.S. Thejas, *J. Electron. Mater.* 51, 938–952 (2022).
36. K. Ramam, M. Lopez, *J. Mater. Sci.: Mater. Electron.* 19, 1140–1145 (2008).
37. T. Badapanda, S. Sarangi, B. Behera, S. Anwar, T. P. Sinha, R. Ranjan, G. E. Luz Jr.,E. Longo, L. S. Cavalcante, *J Mater Sci: Mater. Electron.* 25, 3427–3439 (2014).
38. P.A. Jha, A.K. Jha, *Curr. Appl. Phys.* 13, 1413–1419 (2013).
39. D. Lin, K.W. Kwok, H.L.W. Chan, *Ceram. Int.* 40, 6841–6846 (2014).
40. C.S. Yu, H.L. Hsieh, *J. Eur. Ceram. Soc.* 25, 2425–2427 (2005).
41. Y. Yan, K.H. Cho, S. Priya, *J. Am. Ceram. Soc.* 94, 3953–3959 (2011).
42. P. K. Panda, B. Sahoo, T.S. Thejas, *Sens. Int.* 4, 100226 (2023).
43. J. Hao, W. Li, J. Zhai, H. Chen, *Mater. Sci. Eng. R* 135, 1–57 (2019).
44. F.Z. Yao, J. Glaum, K. Wang, W. Jo, J. Rödel, J.F. Li, *Appl. Phys. Lett.* 103, 192907 (2013).